catalysts

MDPI

Article

Low-Temperature Oxidation of Dimethyl Ether to Polyoxymethylene Dimethyl Ethers over CNT-Supported Rhenium Catalyst

Qingde Zhang [1], Wenfeng Wang [1,2], Zhenzhou Zhang [1,2], Yizhuo Han [1,*] and Yisheng Tan [1,*]

[1] State Key Laboratory of Coal Conversion, Institute of Coal Chemistry, Chinese Academy of Sciences, Taiyuan 030001, China; qdzhang@sxicc.ac.cn (Q.Z.); wangwf@sxicc.ac.cn (W.W.); zhangzz@sxicc.ac.cn (Z.Z.)

[2] Graduate University of Chinese Academy of Sciences, Beijing 100049, China

* Correspondence: hanyz@sxicc.ac.cn (Y.H.); tan@sxicc.ac.cn (Y.T.); Tel./Fax: +86-351-404-4287 (Y.T. & Y.H.); +86-351-404-9747 (Y.T. & Y.H.)

Academic Editor: Stuart H. Taylor

Received: 14 December 2015; Accepted: 3 March 2016; Published: 14 March 2016

Abstract: Due to its excellent conductivity, good thermal stability and large specific surface area, carbon nano-tubes (CNTs) were selected as support to prepare a Re-based catalyst for dimethyl ether (DME) direct oxidation to polyoxymethylene dimethyl ethers (DMM_x). The catalyst performance was tested in a continuous flow type fixed-bed reactor. $H_3PW_{12}O_{40}$ (PW_{12}) was used to modify Re/CNTs to improve its activity and selectivity. The effects of PW_{12} content, reaction temperature, gas hourly space velocity (GHSV) and reaction time on DME oxidation to DMM_x were investigated. The results showed that modification of CNT-supported Re with 30% PW_{12} significantly increased the selectivity of DMM and DMM_2 up to 59.0% from 6.6% with a DME conversion of 8.9%; besides that, there was no CO_x production observed in the reaction under the optimum conditions of 513 K and 1800 h^{-1}. The techniques of XRD, BET, NH_3-TPD, H_2-TPR, XPS, TEM and SEM were used to characterize the structure, surface properties and morphology of the catalysts. The optimum amount of weak acid sites and redox sites promotes the synthesis of DMM and DMM_2 from DME direct oxidation.

Keywords: dimethyl ether; low-temperature oxidation; polyoxymethylene dimethyl ethers; carbon nano-tubes; Re; $H_3PW_{12}O_{40}$

1. Introduction

Dimethyl ether (CH_3OCH_3, DME) is a clean fuel with high cetane number and is also a potential and non-petroleum route chemical synthesis material. DME can be synthesized via one-step process at low cost from syngas generated from coal, biomass and natural gas. Because of the low boiling point of DME (246.3 K), it is not possible to simply replace diesel with DME or directly blend DME with diesel. Polyoxymethylene dimethyl ethers ($CH_3O(CH_2O)_xCH_3$, DMM_x) are promising diesel oil additives due to the similar structure of –C–O–C–O–C–O–C– with DME and high content of oxygen and cetane number [1]. The addition of DMMx to diesel oil can greatly improve the combustion and reduce particular matter emissions of diesel engines. In indusry, DMM_x is mainly produced via condensation of methanol and trioxymethylene over acidity catalysts [2], but this synthesis technology has the problems of high energy consumption, high investment and high operation cost. Utilizing oxidation of DME to synthesize DMM_x is one of the most attractive green routes for the synthesis of clean fuel additives with a short process, low CO_2 emissions and high energy efficiency.

DME oxidation has been paid more and more attention due to the advantages of simplicity and feasibility [3–8]. Yagita Hirosh *et al.* examined DME oxidation to 1,2-dimethoxyethane (DMET) over a SnO_2/MgO catalyst [9]. Wenjie Shen *et al.* investigated the supported MoO_x and VO_x catalysts

for DME oxidation to HCHO [10]. Haichao Liu *et al.* reported that the synthesis of DMM from the oxidation of DME and methanol using $H_{3+n}V_nMo_{12-n}PO_{40}$ [11]. In recent years, our group has been focusing on the selective oxidation of DME to HCHO, methyl formate (MF), DMM_x, *etc.* over different catalysts [12–15].

In our previous work, a Mn-(Sm+SiW_{12})/SiO_2 catalyst exhibited good activity for the selective oxidation of DME to DMM at 593K, but by-product CO_x was usually formed due to a high reaction temperature [16]. Though the DMM synthesis from DME oxidation has been realized, further enhancing the chain growth of C–O to obtain larger DMM_x molecules from DME direct oxidation at low temperature is still a very challenging task.

Rhenium oxide is widely used in some oxidation reactions due to its unique redox and acidic properties [17–23]. We have also found that Re/TiO_2 was active for the selective oxidation of DME and DMM as co-reactants to DMM_2 [14]; however, the low surface area of TiO_2 affects the dispersion of active components, and catalyst particles are prone to sintering during the reaction, which restrains the increase of catalyst activity. Carbon nano-tubes (CNTs) have been applied as support in catalytic reactions because of their excellent conductivity, good thermal stability and large specific surface area [24–28].

In the present study, CNTs were selected as support due to their unique surface properties. The $H_3PW_{12}O_{40}$ (PW_{12}), which can offer acidity, was used to modify Re/CNTs. The effects of PW_{12} content, reaction temperature, gas hourly space velocity (GHSV), and reaction time on DME oxidation to DMMx were investigated. The results show that the PW_{12}-modified Re/CNTs demonstrates high activity and selectivity for the formation of DMM and DMM_2 via DME direct oxidation at low temperature. The total selectivity of DMM and DMM_2 reaches 59.0% with DME conversion of 8.9% at 513 K without CO_x formation over 5%Re-30%PW_{12}/CNTs. The techniques of XRD, BET, NH_3-TPD, H_2-TPR, XPS, TEM and SEM are used to characterize the structure, surface properties and morphology of the catalysts. Until now, there have been no reports about the DME oxidation to DMM and DMM_2 over CNT-supported Re catalyst.

2. Results and Discussion

2.1. Effects of PW_{12} Content on the Performance of 5%Re-PW_{12}/CNTs

Table 1 shows the selectivity and the conversion of DME as a function of PW_{12} content in 5%Re-PW_{12}/CNTs. Over a CNT-supported Re catalyst, DME conversion is only 4.2%, and DMM selectivity is as low as 6.6% and no DMM_2 is found, but HCHO selectivity reaches 73.7%, which indicates that Re/CNTs exhibits more redox sites than acid sites. When 5%PW_{12} is used to modify Re/CNTs, there is an evident increase in DMM selectivity, and a trace of DMM_2 is formed. After 20%PW_{12} introduction to Re/CNTs, DMM selectivity is clearly increased to 45.9%, and its selectivity reaches 4.1%. The selectivity of DMM and DMM_2 reaches the highest value of 59.0%, and DME conversion is also increased to 8.9% when Re/CNTs is modified by 30%PW_{12}. However, a further increase of PW_{12} content leads to a decline in the selectivity of DMM_{1-2}. Especially, when PW_{12} content reaches as high as 80%, DME is mainly oxidized to CO with 64.4% selectivity. The activity and selectivity of pure 30%PW_{12} before Re addition has been also investigated and the DMM selectivity of 32.7% is obtained; besides that, DMM_2 selectivity reaches 13.9%, but by-product CO is found with the selectivity of 14.6%.

The results show that the addition of PW_{12} has obvious effects on DME conversion and DMM selectivity. It can be seen in Table 1 that no CO_x is formed in the reaction of DME to DMM and DMM_2 when CNTs are used as support along with an optimum amount of PW_{12} introduction under the conditions of 513 K and 1800 h^{-1}. This may be due to the special adsorption capacity and excellent conductivity of CNTs.

Table 1. Effects of PW_{12} content on the performance of 5%Re-PW_{12}/CNTs.

Catalysts	DME Conversion (%)	Selectivity (C-mol%)							
		DMM	DMM_2	CH_3OH	HCHO	MF	CO	CH_4	CO_2
Re/CNTs	4.2	6.6	0	16.2	73.7	3.5	0	0	0
Re-5%PW_{12}/CNTs	4.9	26.3	0.3	2.7	67.7	3.0	0	0	0
Re-20%PW_{12}/CNTs	6.1	45.9	4.1	2.6	45.0	2.4	0	0	0
Re-30%PW_{12}/CNTs	8.9	55.0	4.0	4.2	31.4	5.4	0	0	0
Re-40%PW_{12}/CNTs	9.5	50.7	3.7	4.4	38.9	2.3	0	0	0
Re-80%PW_{12}/CNTs	15.0	27.5	1.7	3.5	2.1	0.8	64.4	0	0
30%PW_{12}/CNTs	10.0	32.7	13.9	16.8	21.4	0.6	14.6	0	0

Reaction conditions: atmospheric pressure, 513 K, cat.: 1 mL, 15 min, 1800 h^{-1}, nO_2:nDME = 1:1.

In our previous work, a possible reaction mechanism of DME oxidation to DMM was proposed and DMM synthesis needed acid sites and redox sites [7,16]. According to the present reaction results, DMM can probably be formed by the acetalization reaction of methanol (formed by DME hydrolysis over acid sites) and HCHO (oxidized by CH_3OH over redox sites) at low temperature. We also suggest that DMM may be the intermediate for the formation of DMM_2 via DME oxidation [14]. $CH_3OCH_2OCH_2OCH_3$ may be synthesized via $CH_3OCH_2OCH_2$ group (obtained after the cleavage of the terminal C–H bond of DMM molecule over the redox sites) combining CH_3O (formed over acid sites) under the cooperation of the acid sites and the redox sites of the catalyst. Therefore, optimum amount of the acid sites and redox sites of the catalyst is beneficial to the formation of DMM and DMM_2 from DME oxidation.

2.2. Effects of Reaction Temperature on the Performance of 5%Re-30%PW_{12}/CNTs

Table 2 shows the effects of reaction temperature on DME conversion and the selectivity of DMM and DMM_2 over 5%Re-30%PW_{12}/CNTs. With increasing reaction temperature, DME conversion keeps an upward trend because DME molecule is easily activated at higher temperatures. At 493 K, the total selectivity of DMM and DMM_2 is 19.8% with DME conversion of 6.6%, but the HCHO selectivity is as high as 62.0%. The selectivity of DMM and DMM_2 reaches the highest value of 59.0%, and HCHO selectivity clearly decreases to 31.4% when temperature is increased to 513 K. Then, the selectivity of DMM and DMM_2 decreases constantly with the increase in temperature. At 533 K, the selectivity of DMM and DMM_2 decreases to 49.8%, and, concurrently, by-product CO appears and its selectivity is 13.2%. CO selectivity reaches 21.9% when temperature is further increased to 553 K. Lower temperature is not the optimum conditions for DME oxidation to DMM and DMM_2, and HCHO is the main by-product. However, higher temperature easily leads to over-oxidation of DME to produce more CO. Therefore, the optimum reaction temperature is 513 K for DME direct-oxidation to DMM and DMM_2 with high DMM_{1-2} selectivity and low by-product selectivity.

Table 2. Effects of reaction temperature on the performance of 5%Re-30%PW_{12}/CNTs.

Reaction Temperature (K)	DME Conversion (%)	Selectivity (C-mol%)							
		DMM	DMM_2	CH_3OH	HCHO	MF	CO	CH_4	CO_2
493	6.6	17.0	2.8	16.5	62.0	1.7	0	0	0
513	8.9	55.0	4.0	4.2	31.4	5.4	0	0	0
533	10.9	45.7	4.1	4.1	31.1	1.8	13.2	0	0
553	12.3	43.8	3.7	3.9	26.0	0.7	21.9	0	0

Reaction conditions: atmospheric pressure, cat.: 1 mL, 15 min, 1800 h^{-1}, nO_2:nDME = 1:1.

2.3. Effects of Gas Hourly Space Velocity on the Performance of 5%Re-30%PW_{12}/CNTs

The effects of GHSV on DME oxidation to DMM_{1-2} over 5%Re-PW_{12}/CNTs are shown in Table 3. As can be seen in Table 3, CH_3OH and HCHO are the main products when GHSV is lower, while the higher GHSV results in higher HCHO selectivity. When GHSV is 1200 h^{-1}, CH_3O^- from DME decomposition tends to adsorb on the acid sites of the catalyst, then CH_3OH is formed and concurrently is partly oxidized to HCHO over redox sites, so CH_3OH and HCHO formed as the main by-products. HCHO easily desorbs from the catalyst surface and has less opportunity to react with methanol to form DMM_{1-2} when GHSV is higher than 1800 h^{-1}. It is proposed that HCHO may be the intermediate of DMM and DMM_2 formation via DME direct oxidation. At a GHSV of 1800 h^{-1}, DMM_{1-2} selectivity reaches a maximum of 59.0%.

Table 3. Effects of GHSV on the performance of 5%Re-30%PW_{12}/CNTs.

GHSV (h^{-1})	DME Conversion (%)	Selectivity (C-mol%)							
		DMM	DMM_2	CH_3OH	HCHO	MF	CO	CH_4	CO_2
1200	9.8	28.3	2.0	28.2	34.2	7.3	0	0	0
1800	8.9	55.0	4.0	4.2	31.4	5.4	0	0	0
2400	5.0	35.7	5.1	8.8	50.4	0	0	0	0
3000	3.4	34.9	0.1	9.3	55.7	0	0	0	0

Reaction conditions: atmospheric pressure, 513 K, cat.: 1 mL, 15 min, nO_2:nDME = 1:1.

2.4. Effects of Reaction Time on the Performance of 5%Re-30%PW_{12}/CNTs

The effects of reaction time on the conversion of DME and the selectivities of the main products over the 5%Re-30%PW_{12}/CNTs catalyst were investigated. As can be seen in Figure 1, the total selectivity of DMM and DMM_2 reaches 59.0% at 15 min. There is a slight decrease from 59.0% to 49.3% in the selectivity of DMM and DMM_2, and DME conversion has no obvious changes during the 300-min reaction. The 5%Re-30%PW_{12}/CNTs catalyst exhibits high initial activity.

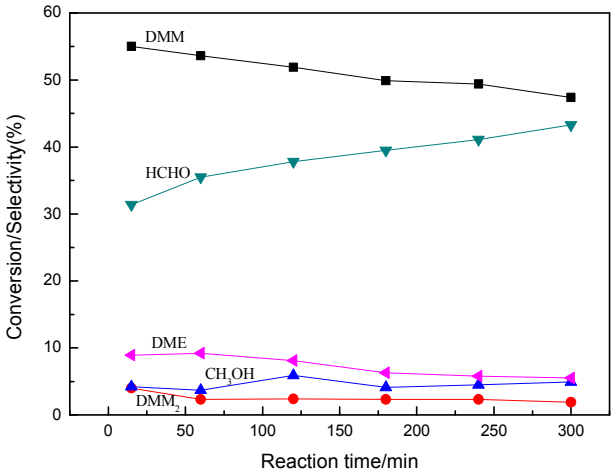

Figure 1. Effects of reaction time on the performance of 5%Re-30%PW_{12}/CNTs.

2.5. Catalyst Characterization

2.5.1. XRD

Figure 2 shows the XRD patterns of CNT-supported Re catalysts with different PW_{12} content. For the Re/CNTs catalyst, only diffraction peaks of CNTs exist and no peaks of Re oxides are found, indicating that Re oxides are highly dispersed on the catalyst surface. When 20%PW_{12} is introduced to

Re/CNTs, the diffraction peaks of PW_{12} appear, and the intensity of the peak becomes stronger, while the diffraction peaks of CNTs become weaker with the increase of PW_{12} content.

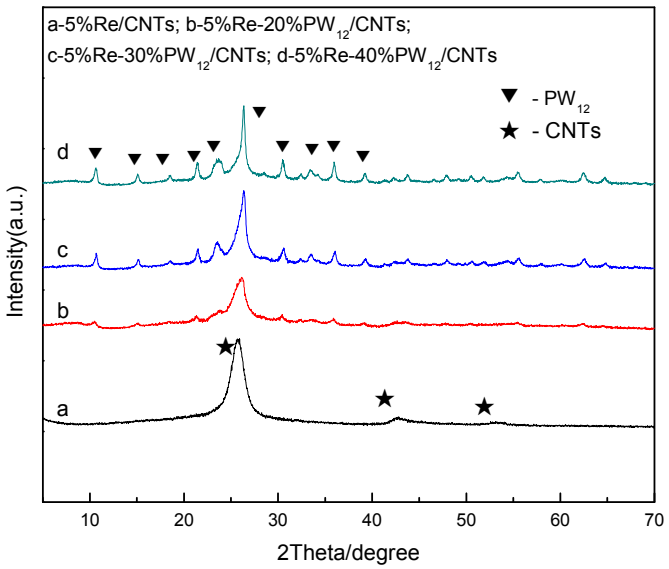

Figure 2. XRD profiles of 5%Re-PW_{12}/CNTs with different PW_{12} content.

2.5.2. BET Surface Area

Table 4 shows the textural properties of CNT-supported catalysts. 5%Re/CNTs have much larger surface area than other catalysts. 30%PW_{12} introduction decreases the BET surface area of 5%Re/CNTs from 217.4 to 90.9 $m^2 \cdot g^{-1}$ and leads to a decrease in the pore volume. It appears more obvious that the BET surface area of the catalyst decreases to 15.2 $m^2 \cdot g^{-1}$ sharply, and the pore volume is only as low as 0.062 $cm^3 \cdot g^{-1}$ when 80% PW_{12} is introduced to Re/CNTs. This may be due to the pore blockage and the surface coverage by excessive PW_{12}. It can be seen in Table 4 that the BET surface area of the 5%Re-30%PW_{12}/CNTs catalyst decreases from 90.9 to 81.1 $m^2 \cdot g^{-1}$ 6 h post-reaction.

Table 4. Textural properties of the catalysts.

Catalysts	BET Surface Area A ($m^2 \cdot g^{-1}$)	Total Pore Volume v ($cm^3 \cdot g^{-1}$)	Average Pore Diameter d (nm)
5%Re/CNTs	217.4	1.054	19.399
5%Re-30%PW_{12}/CNTs	90.9	0.467	20.539
5%Re-30%PW_{12}/CNTs after reaction	81.1	0.523	25.795
5%Re-80%PW_{12}/CNTs	15.2	0.062	16.402

2.5.3. NH_3-TPD

Figure 3 shows the NH_3-TPD profiles of 5%Re-PW_{12}/CNTs with different PW_{12} content. Re/CNTs only has weak acid sites due to an NH_3 desorption peak at about 430 K. When PW_{12} was introduced into Re/CNTs, two NH_3 desorption peaks at about 470 and 630 K, corresponding to weak acid sites and strong acid sites, appeared respectively. In order to compare the changes of acid sites after PW_{12} introduction, the area of NH_3 desorption peaks were integrated (see Table 5). By increasing the content of PW_{12}, the number of the weak acid sites and the strong acid sites becomes larger. The ratio of S1(weak acid sites)/S2(strong acid sites) is highest when PW_{12} content is 30%. According to the reaction results, the increased amount of weak acid sites can favor the formation of DMM and DMM_2 from DME oxidation.

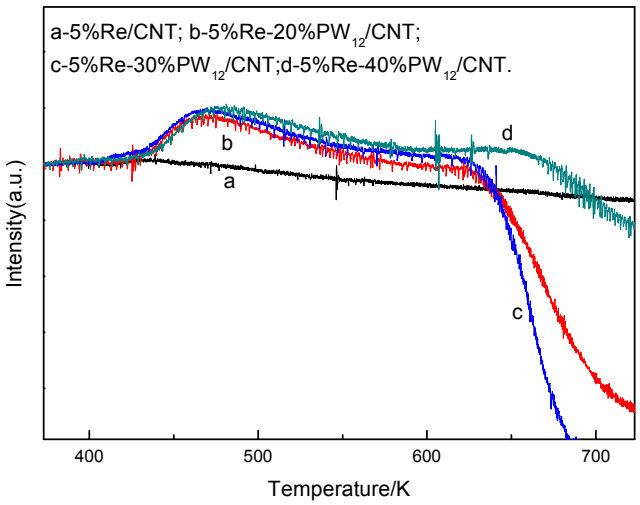

Figure 3. NH_3-TPD profiles of 5%Re-PW_{12}/CNTs with different PW_{12} content.

Table 5. Results of NH_3-TPD integration.

Catalysts	Weak Acid Sites Area(S1)	Strong Acid Sites Area(S2)	Ratio S1/S2
5%Re/CNTs	100	-	-
5%Re-20%PW_{12}/CNTs	89.8	10.2	8.8
5%Re-30%PW_{12}/CNTs	90.0	10.0	9.0
5%Re-40%PW_{12}/CNTs	86.9	13.1	6.6

2.5.4. H_2-TPR

Figure 4 shows H_2-TPR profiles of 5%Re-PW_{12}/CNTs with different PW_{12} content. For the Re/CNTs catalyst, the peaks for H_2 consumption appear at about 638 K. An evident shift to lower temperature is observed after the introduction of PW_{12} into Re/CNTs, suggesting that the addition of PW_{12} can significantly facilitate the reduction of Re oxide species. When the PW_{12} content is 30%, the temperature of reduction peak reaches its lowest value at 509 K, which suggests that 5%Re-30%PW_{12}/CNTs exhibit strong redox ability. The interaction of PW_{12} and the surface Re species increases the reducibility of Re-PW_{12}/CNTs, consistent with the results of the introduction of PO_4^{3-} and SO_4^{2-}, affecting the reducibility of VO_x/TS-1 [29].

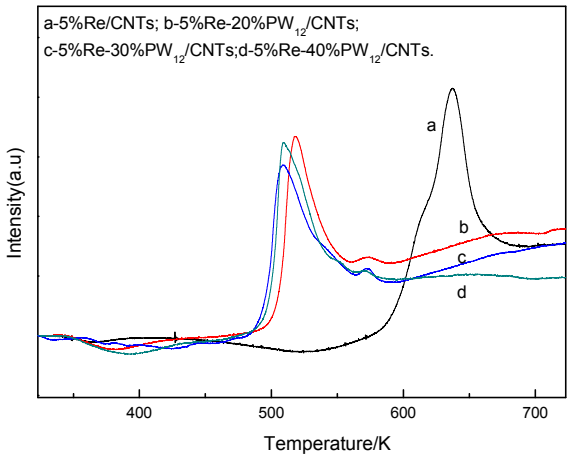

Figure 4. H_2-TPR profiles of 5%Re-PW_{12}/CNTs with different PW_{12} content.

2.5.5. XPS

Figure 5 shows the Re 4f and O1s XPS spectra of the 5%Re/CNTs and 5%Re-30%PW_{12}/CNTs catalysts. In contrast, a peak at 45.6 eV is found over the 5%Re/CNTs catalyst, which should ascribe to the Re $4f_{7/2}$ level for Re^{7+} species, indicating that Re^{7+} species were mainly present on the surface of Re/CNTs [20,23]. However, in our previous XPS study, Re^{7+} was observed at 46.6eV over 5%Re/TiO_2. This also indicates that the existence form of Re species changes due to the different interaction of Re and support. However, when PW_{12} is introduced to Re/CNTs, the most remarkable change is the appearance of a peak at 41.9 eV assigned to Re^{4+} species [20,23]. This suggests a strong interaction between Re oxide species and the surface of CNTs in line with the results of TPR, which indicates that the introduction of PW_{12} evidently changes the surface properties of CNTs and further facilitates the formation of Re^{4+} species. Additionally, the intensity of O1s has an obvious change before and after PW_{12} introduction. This further proves that the species of Re oxides are changed by PW_{12}. Combined with the reaction results, the presence of both Re^{4+} and Re^{7+} species are further proved to promote the formation of DMM and DMM_2.

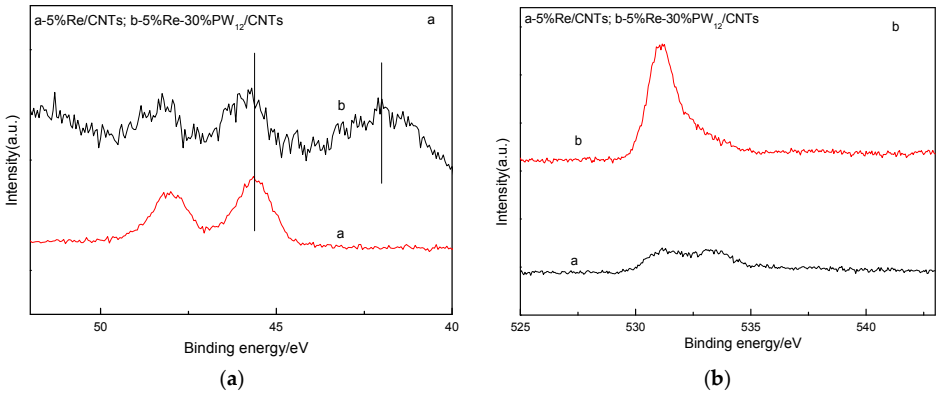

Figure 5. Re 4f (**a**) and O1s; (**b**) XPS spectra for 5%Re/CNTs and 5%Re-30%PW_{12}/CNTs.

2.5.6. TEM

Figure 6 demonstrates the TEM images of 5%Re/CNTs, 5%Re-30%PW_{12}/CNTs before and after the catalytic oxidation of DME at 513 K and 5%Re-80%PW_{12}/CNTs. Figure 6 conveys that there are distinctive differences in the images between 5%Re/CNTs and 5%Re-30%PW_{12}/CNTs catalysts. Over 5%Re/CNTs, no ReO_x is found due to highly dispersed Re species over the surface of CNTs. It can be seen that the inner pores of CNTs are filled with PW_{12} after 30%PW_{12} introduction, and, especially, ReO_x particles are clearly found over the outer surface of CNTs and the particle size of ReO_x is about 0.7 nm. After reaction, the sample shows some agglomeration of PW_{12} and Re species. When PW_{12} content is increased to 80%, excessive PW_{12} clearly deposits not only on the inner surface, but also the outer surface of CNTs.

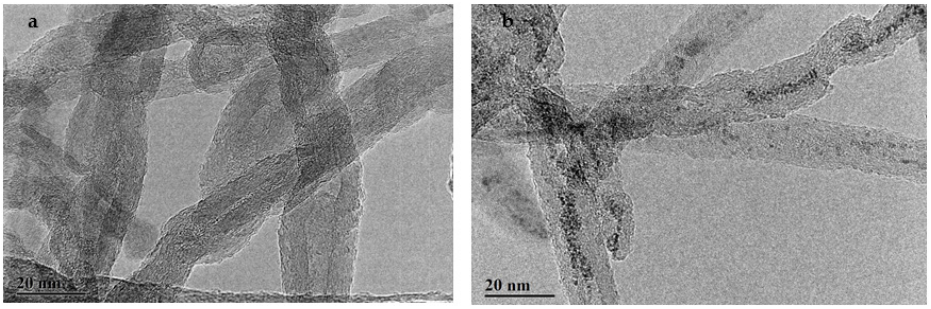

Figure 6. *Cont.*

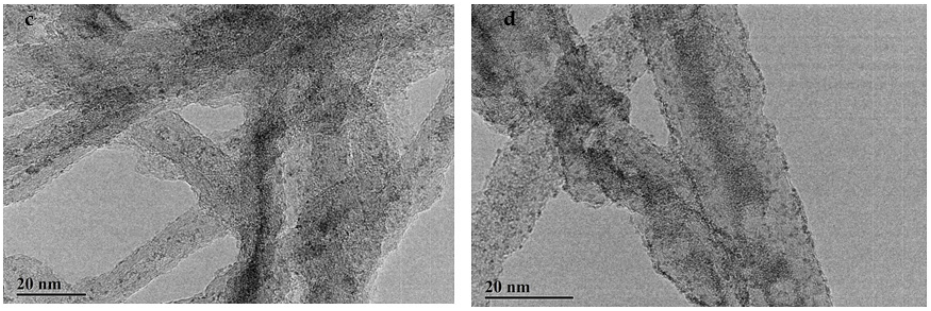

Figure 6. TEM images of 5%Re/CNTs (**a**); 5%Re-30%PW_{12}/CNTs (**b**); 5%Re-30%PW_{12}/CNTs 6 h post-reaction (**c**) and 5%Re-80%PW_{12}/CNTs (**d**).

2.5.7. SEM

The SEM micrographs of 5%Re/CNTs, 5%Re-30%PW_{12}/CNTs, 5%Re-30%PW_{12}/CNTs 6 h post-reaction and 5%Re-80%PW_{12}/CNTs catalysts are demonstrated in Figure 7. It can be seen in Figure 7 that PW_{12} also exists over the outer surface of CNTs (TEM has proved that PW_{12} can enter the inner surface of CNTs) after 30%PW_{12} introduction to Re/CNTs. After reaction, the catalyst particles tend to aggregate, leading to the decrease of BET surface area (Table 4). In evidence, PW_{12} and CNTs agglomerated almost completely due to the excessive introduction of PW_{12} (80%PW_{12}). Combined with the TEM results, PW_{12} prefers to enter the inner pores of CNTs when PW_{12} content is low, while PW_{12} mainly deposits on the outer surface of CNTs along with the increase of PW_{12} content.

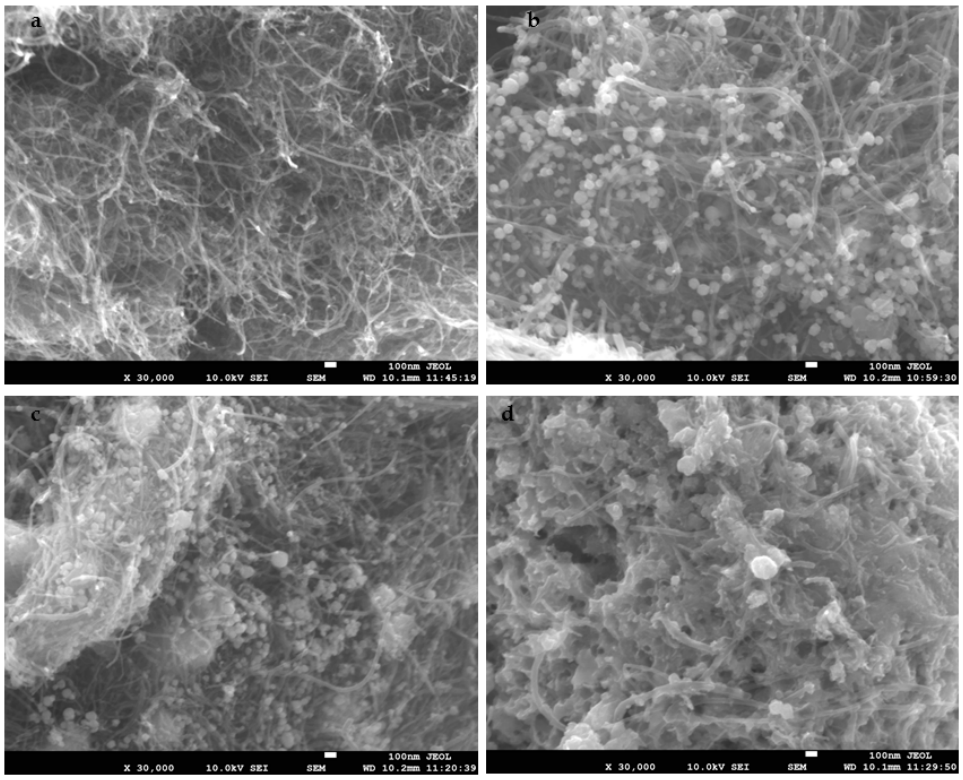

Figure 7. SEM images of 5%Re/CNTs (**a**); 5%Re-30%PW_{12}/CNTs (**b**); 5%Re-30%PW_{12}/CNTs 6 h post-reaction (**c**) and 5%Re-80%PW_{12}/CNTs (**d**).

For the 5%Re/CNTs catalyst, ReO_x is dispersed uniformly on the surface of CNTs according to the results of XRD and TEM. According to the results of XPS, Re species mainly exists in the form of

Re_2O_7. After PW_{12} introduction to Re/CNTs, PW_{12} dispersed on the inner and outer surface of CNTs and affected the dispersion of ReO_x on the surface of CNTs. The introduction of optimum amount of PW_{12} not only increased the total amount of acid sites, but also significantly changed the oxidation state of Re species and facilitated the formation of Re^{4+} species. The characterization of the catalysts before and after reaction indicated that the agglomeration of active species may be the main reasons of the catalyst deactivation.

Due to the high stability of the DME molecule, the activation of DME molecule at lower temperature is very difficult, while a higher temperature easily leads to the bond-breaking of C–O and C–H concurrently, and further results in the complex products along with CO_x production. Therefore, how to activate DME at a lower temperature and selectively convert DME to target chemicals without CO_x formation is a challenging task. DMM_x selectivity is a very important factor for the DME highly selective oxidation to a diesel oil additive. The higher DMM_x selectivity is, the better DME utilization is, provided that no CO_x is produced during DME oxidation reactions. As the main products, DMM_x, HCHO and CH_3OH can be separated by distillation according to their different boiling points. In the present work, the low-temperature oxidation of DME to DMM_x with high DMM_x selectivity of 59.0% and DME conversion of 8.9% was realized with no CO_x production over the 5%Re-30%PW_{12}/CNTs. We should manage to increase DMM_x selectivity in our future work based on previous results. The conversion of DME is not too high, but increasing the DME conversion easily leads to more by-products. For the 5%Re-30%PW_{12}/CNTs catalyst, enhancing the PW_{12} content, increasing reaction temperature and decreasing GHSV can raise the DME conversion; however, DMM_x selectivity decreases clearly, and CO_x is also produced. Combining the reaction results, the 5%Re-30%PW_{12}/CNTs catalyst has some advantages if it can be used in the related field in the future. The reaction temperature is 80 K lower than that reported in our previous work; more importantly, no CO_x was formed over 5%Re-30%PW_{12}/CNTs. Additionally, the catalyst stability was also increased, compared to the catalyst in the previous work. Though the once-through DME conversion is not very high, the unconverted DME can be recycled to improve its utilization. These promising results can help us thoroughly understand the reaction mechanism of DME activation and offer further possible industrial applications in the future.

3. Experimental Section

3.1. Catalyst Preparation

$H_3PW_{12}O_{40}$-modified Re/CNTs catalysts were prepared by the incipient wetness impregnation method. An aqueous solution of $H_3PW_{12}O_{40}$ (Shanghai Chemical Co., Shanghai, China) was impregnated in CNTs ((Multi-walled carbon nanotubes, inner diameter = 4–8 nm, outer diameter <10–20 nm, Chengdu Organic Chemicals Co. Ltd., Chengdu, China). Raw CNTs were refluxed in HNO_3 (68 wt. %) for 14 h at 140 °C in an oil bath; then the mixture was filtered and washed with deionized water, followed by drying at 60 °C for 12 h.) at 298 K for 6 h, then dried overnight at 393 K, and calcined at 673 K for 4 h. An aqueous solution of ammonium perrhenate (NH_4ReO_4, Strem Chemicals, Inc., Newburyport, MA, USA) was used to impregnate the $H_3PW_{12}O_{40}$/CNTs, and the following procedures were the same as the above. The catalyst was designated as 5%Re-20%PW_{12}/CNTs, 5%Re-30%PW_{12}/CNTs, and 5%Re-40%PW_{12}/CNTs. Re/CNTs was prepared according to the above procedures. For the catalysts used in this study, Re and PW_{12} refer to Re_2O_7 and $H_3PW_{12}O_{40}$, respectively. The amount of Re in the catalyst refers to the amount of Re_2O_7.

3.2. Catalytic Oxidation of DME

The catalytic oxidation of DME was carried out in a continuous flow type fixed-bed reactor. The catalyst (1 mL, 20–40 mesh) was diluted with ground quartz to prevent the over-heating of the catalyst due to exothermic reaction. The catalyst was treated in flow of O_2 (30 mL/min) for 1 h before reaction. The reactant mixture consisted of DME and O_2 with ratio of nO_2:nDME = 1:1. The reaction products were analyzed by gas chromatography GC-2014CPF/SPL (Shimadzu Co., Kyoto, Japan)

equipped with a flame ionization detector (60 m × 0.25 mm, DB-1 column, Agilent Technologies Inc., Palo Alto, IA, USA) and GC-2014 (Shimadzu Co., Kyoto, Japan) with a thermal conductivity detector (Porapak T column, Waters Corporation, Milford, MA, USA). GC-4000A (TDX-01 column, East & West Analytical Instruments, Inc., Beijing, China) with thermal conductivity detectors was used to analyze H_2, CO, CO_2 and CH_4.

The data of the whole work was calculated based on carbon balance, and the carbon balances of most experiments were within 95%–99%.

3.3. Structure and Properties Characterization

3.3.1. BET Surface Area

Surface areas of the samples were measured by a BET nitrogen adsorption method at 77.35 K using a TriStar 300 machine (Micromeritics, Atlanta, GA, USA). The samples were treated at 473 K under vacuum conditions for 8 h before BET test.

3.3.2. X-ray Diffraction (XRD)

XRD patterns were measured on a Bruker Advanced X-Ray Solutions/D8-Advance (Bruker, Karlsruhe, Germany) using Cu Ka radiation. The anode was operated at 40 kV and 40 mA. The 2-Theta angles were scanned from 5° to 70°.

3.3.3. Temperature Programmed Desorption (TPD)

The NH_3-TPD profiles were obtained in a fixed-bed reactor system connected with a thermal conductivity detector (Tianjin Xianquan Co. Ltd., Tianjin, China). The catalyst sample (100 mg) was pretreated at 673 K under N_2 flow (40 mL/min) for 2 h and then cooled down to 373 K under N_2 flow. Then NH_3 of 40 mL/min was introduced into the flow system for a continuous 20 min before doing TPD. The dose amount of NH_3 maintained the same for all the samples investigated. The TPD profiles were recorded at a temperature rising rate of 5 K/min from 373 to 923 K.

3.3.4. Temperature Programmed Reduction (TPR)

H_2-TPR was conducted in a fixed-bed reactor system equipped with a thermal conductivity detector (Tianjin Xianquan Co. Ltd., Tianjin, China). The sample (100 mg) was pretreated in Ar at 673 K for 0.5 h and then cooled down to 323 K. After that, a 10%H_2/Ar mixed gas was switched on and the temperature was increased linearly at a rate of 5 K/min from 323 K to 923 K.

3.3.5. X-ray Photoelectron Spectra (XPS)

XPS were measured on a XPS-AXIS Ultra of Kratos Co. (Manchester, UK) by using Mg Ka radiation (Hν = 1253.6 eV) with X-ray power of 225 W (15 kV, 15 mA).

3.3.6. Transmission Electron Microscope (TEM)

TEM images were taken on a JEM-2010 Transmission electron microscope (JEOL Company, Tokyo, Japan).

3.3.7. Scanning Electron Microscope (SEM)

SEM images were taken on a JSM-35C scanning electron microscope (JEOL Company, Tokyo, Japan) operated at 25 kV.

4. Conclusions

Low-temperature oxidation of DME to DMM and DMM_2 was successfully realized over a CNT-supported Re-based catalyst. The introduction of PW_{12} markedly increases the activity of

Re/CNTs. The total selectivity of DMM and DMM_2 reaches 59.0% with DME conversion of 8.9% at 513 K without the formation of CO_x over 5%Re-30%PW_{12}/CNTs. CNTs as support play an important role in promoting the synthesis of DMM_x and inhibiting the formation of CO_x due to its unique physical and chemical properties.

Acknowledgments: This work was supported by the National Natural Science Foundation of China (No. 21373253, No. 20903114) and Youth Innovation Promotion Association CAS (No. 2014155).

Author Contributions: Qingde Zhang performed experiments and wrote the paper; Wenfeng Wang and Zhenzhou Zhang characterized the catalysts; Yisheng Tan and Yizhuo Han conceived the experiments and revised the paper.

Conflicts of Interest: The authors declare no conflict of interest.

References

1. Wu, J.B.; Zhu, H.Q.; Wu, Z.W.; Qin, Z.F.; Yan, L.; Du, B.L.; Fan, W.B.; Wang, J.G. High Si/Al ratio HZSM-5 zeolite: An efficient catalyst for the synthesis of polyoxymethylene dimethyl ethers from dimethoxymethane and trioxymethylene. *Green Chem.* **2015**, *17*, 2353–2357. [CrossRef]
2. Zhao, Q.; Wang, H.; Qin, Z.F.; Wu, Z.W.; Wu, J.B.; Fan, W.B.; Wang, J.G. Synthesis of polyoxymethylene dimethyl ethers from methanol and trioxymethylene with molecular sieves as catalysts. *J. Fuel Chem. Tech.* **2011**, *39*, 918–923. [CrossRef]
3. Liu, H.C.; Cheung, P.; Iglesia, E. Structure and support effects on the selective oxidation of dimethyl ether to formaldehyde catalyzed by MoO_x domains. *J. Catal.* **2003**, *217*, 222–232. [CrossRef]
4. Guo, H.J.; Sun, W.T.; Haas, F.M.; Farouk, T.; Dryer, F.L.; Ju, Y.G. Measurements of H_2O_2 in low temperature dimethyl ether oxidation. *P. Combust. Inst.* **2013**, *34*, 573–581. [CrossRef]
5. Liu, H.C.; Iglesia, E. Selective oxidation of dimethyl ether to formaldehyde on small molybdenum oxide domains. *J. Catal.* **2002**, *208*, 1–5. [CrossRef]
6. Yu, L.; Xu, J.Y.; Sun, M.; Wang, X.T. Catalytic oxidation of dimethyl ether to hydrocarbons over SnO_2/MgO and SnO_2/CaO catalysts. *J. Nat. Gas. Chem.* **2007**, *16*, 200–203. [CrossRef]
7. Zhang, Q.D.; Tan, Y.S.; Yang, C.H.; Han, Y.Z. $MnCl_2$ modified $H_4SiW_{12}O_{40}/SiO_2$ catalysts for catalytic oxidation of dimethyl ether to dimethoxymethane. *J. Mole. Catal. A* **2007**, *263*, 149–155. [CrossRef]
8. Liu, G.B.; Zhang, Q.D.; Han, Y.Z.; Tsubaki, N.; Tan, Y.S. Selective oxidation of dimethyl ether to methyl formate over trifunctional MoO_3-SnO_2 catalyst under mild conditions. *Green Chem.* **2013**, *15*, 1501–1504. [CrossRef]
9. Yagita, H.; Asami, K.; Muramatsu, A. Oxidative dimerization of dimethyl ether with solid catalysts. *Appl. Catal.* **1989**, *53*, L5–L9. [CrossRef]
10. Huang, X.M.; Liu, J.L.; Chen, J.L.; Xu, Y.D.; Shen, W.J. Mechanistic study of selective oxidation of dimethyl ether to formaldehyde over alumina-supported molybdenum oxide catalyst. *Catal. Lett.* **2006**, *108*, 79–86. [CrossRef]
11. Liu, H.C.; Iglesia, E. Selective One-Step Synthesis of dimethoxymethane via methanol or dimethyl ether oxidation on $H_{3+n}V_nMo_{12-n}PO_{40}$ Keggin Structures. *J. Phys. Chem. B* **2003**, *107*, 10840–10847. [CrossRef]
12. Liu, G.B.; Zhang, Q.D.; Han, Y.Z.; Tsubaki, N.; Tan, Y.S. Effects of MoO_3 structure of Mo-Sn catalysts on dimethyl ether oxidation to methyl formate under mild conditions. *Green Chem.* **2015**, *17*, 1057–1064. [CrossRef]
13. Zhang, Z.Z.; Zhang, Q.D.; Jia, L.Y.; Wang, W.F.; Zhang, T.; Han, Y.Z.; Tsubaki, N.; Tan, Y.S. Effects of tetrahedral molybdenum oxide species and MoO_x domains on the selective oxidation of dimethyl ether under mild conditions. *Catal. Sci. Technol.* **2016**. [CrossRef]
14. Zhang, Q.D.; Tan, Y.S.; Liu, G.B.; Zhang, J.F.; Han, Y.Z. Rhenium oxide modified $H_3PW_{12}O_{40}/TiO_2$ catalysts for selective oxidation of dimethyl ether to dimethoxy dimethyl ether. *Green Chem.* **2014**, *16*, 4708–4715. [CrossRef]
15. Zhang, Q.D.; Tan, Y.S.; Yang, C.H.; Han, Y.Z. Research on catalytic oxidation of dimethyl ether to dimethoxymethane over $MnCl_2$ modified heteropolyacid catalysts. *Catal. Commun.* **2008**, *9*, 1916–1919. [CrossRef]

16. Zhang, Q.D.; Tan, Y.S.; Liu, G.B.; Yang, C.H.; Han, Y.Z. Promotional effects of Sm_2O_3 on Mn-$H_4SiW_{12}O_{40}/SiO_2$ catalyst for dimethyl ether direct-oxidation to dimethoxymethane. *J. Ind. Eng. Chem.* **2014**, *20*, 1869–1874. [CrossRef]
17. Liu, H.C.; Gaigneaux, E.M.; Imoto, H.; Shido, T.; Iwasawa, Y. Novel Re-Sb-O catalysts for the selective oxidation of isobutene and isobutylene. *Appl. Catal. A* **2000**, *202*, 251–264. [CrossRef]
18. Yuan, Y.Z.; Liu, H.C.; Imoto, H.; Shido, T.; Iwasawa, Y. Performance and characterization of a new crystalline $SbRe_2O_6$ catalyst for selective oxidation of methanol to methylal. *J. Catal.* **2000**, *195*, 51–61. [CrossRef]
19. Salameh, A.; Joubert, J.; Baudouin, A.; Lukens, W.; Delbecq, F.; Sautet, P.; Basset, J.M.; Coperet, C. CH_3ReO_3 on γ-Al_2O_3: Understanding its structure, initiation, and reactivity in olefin metathesis. *Angew. Chew. Int. Edit.* **2007**, *46*, 3870–3873. [CrossRef] [PubMed]
20. Yuan, Y.Z.; Iwasawa, Y. Performance and characterization of supported rhenium oxide catalysts for selective oxidation of methanol to methylal. *J. Phys. Chem. B* **2002**, *106*, 4441–4449. [CrossRef]
21. Kusakari, T.; Sasaki, T.; Iwasawa, Y. Selective oxidation of benzene to phenol with molecular oxygen on rhenium/zeolite catalysts. *Chem. Commun.* **2004**, *8*, 992–993. [CrossRef] [PubMed]
22. Yuan, Y.Z.; Shido, T.; Iwasawa, Y. The new catalytic property of supported rhenium oxides for selective oxidation of methanol to methylal. *Chem. Commun.* **2000**, *15*, 1421–1422. [CrossRef]
23. Nikonova, O.A.; Capron, M.; Fang, G.; Faye, J.; Mamede, A.S.; Jalowiecki-Duhamel, L.; Dumeignil, F.; Seisenbaeva, G.A. Novel approach to rhenium oxide catalysts for selective oxidation of methanol to DMM. *J. Catal.* **2011**, *279*, 310–318. [CrossRef]
24. Zhang, F.; Ren, P.J.; Pan, X.L.; Liu, J.Y.; Li, M.R.; Bao, X.H. Self-Assembly of atomically thin and unusual face-centered cubic Re nanowires within carbon nanotubes. *Chem. Mater.* **2015**, *27*, 1569–1573. [CrossRef]
25. Ugarte, D.; Chatelain, A.; DeHeer, W.A. Nanocapillarity and chemistry in carbon nanotubes. *Science* **1996**, *274*, 1897–1899. [CrossRef]
26. Castillejos, E.; Debouttiere, P.J.; Roiban, L.; Solhy, A.; Martinez, V.; Kihn, Y.; Ersen, O.; Philippot, K.; Chaudret, B.; Serp, P. An efficient strategy to drive nanoparticles into carbon nanotubes and the remarkable effect of confinement on their catalytic performance. *Angew. Chem. Int. Edit.* **2009**, *48*, 2529–2533. [CrossRef] [PubMed]
27. Zhang, F.; Pan, X.L.; Hu, Y.F.; Yu, L.; Chen, X.Q.; Jiang, P.; Zhang, H.B.; Deng, S.B.; Bolin, J.T.B.; Zhang, S.; *et al*. Tuning the redox activity of encapsulated metal clusters via the metallic and semiconducting character of carbon nanotubes. *P. Natl. Acad. Sci. USA* **2013**, *110*, 14861–14866. [CrossRef] [PubMed]
28. Qi, W.; Su, D.S. Metal-free carbon catalysts for oxidative dehydrogenation reactions. *ACS Catal.* **2014**, *4*, 3212–3218. [CrossRef]
29. Chen, S.; Wang, S.P.; Ma, X.B.; Gong, J.L. Selective oxidation of methanol to dimethoxymethane over bifunctional VO_x/TS-1 catalysts. *Chem. Commun.* **2011**, *47*, 9345–9347. [CrossRef] [PubMed]